



**Environmental
Science**
Water Research & Technology

**Functionalized electrospun polymer nanofibers for
treatment of water contaminated with uranium**

Journal:	<i>Environmental Science: Water Research & Technology</i>
Manuscript ID	EW-ART-09-2019-000834.R1
Article Type:	Paper

SCHOLARONE™
Manuscripts

Water Impact Statement:

Resource-constrained communities that rely on unregulated water supplies often have limited access to appropriate treatment technologies. Uranium contamination poses a particular challenge for many such communities in the Southwestern United States from legacy mining activities. Here, using insights from uranium extraction efforts, we produce nanotechnology-enabled filtration materials tailored for uranium removal under conditions suitable for point-of-use treatment.

FUNCTIONALIZED ELECTROSPUN POLYMER NANOFIBERS FOR TREATMENT OF WATER CONTAMINATED WITH URANIUM

Adam Johns,¹ Jiajie Qian,¹ Margaret E. Carolan,¹ Nabil Shaikh,² Allison Peroutka,³ Anna Seeger,¹ José M. Cerrato,² Tori Z. Forbes,^{4*} and David M. Cwiertny^{1,3,5*}

¹Department of Civil and Environmental Engineering, University of Iowa, 4105 Seamans Center for the Engineering Arts and Sciences, Iowa City, IA 52242

² Department of Civil, Construction & Environmental Engineering, University of New Mexico, Albuquerque, NM 87131

³Department of Chemical and Biochemical Engineering, University of Iowa, 4133 Seamans Center for the Engineering Arts and Sciences, Iowa City, IA 52242

⁴Department of Chemistry, University of Iowa, Iowa City, IA 52242

⁵Center for Health Effects of Environmental Contamination, 251 North Capitol Street, Chemistry Building - Room W195, The University of Iowa, Iowa City, Iowa 52242

*Co-corresponding authors

DMC: Phone (319) 335-1401; e-mail: david-cwiertny@uiowa.edu

TZF: (319) 384-1320 tori-forbes@uiowa.edu

November 24, 2019

Revised manuscript submitted to *Environmental Science: Water Research & Technology*

ABSTRACT

1
2 Uranium (U) contamination of drinking water often affects communities with limited
3 resources, presenting unique technology challenges for U^{6+} treatment. Here, we develop a suite
4 of chemically functionalized polymer (polyacrylonitrile; PAN) nanofibers for low pressure
5 reactive filtration applications for U^{6+} removal. Binding agents with either nitrogen-containing or
6 phosphorous-based (e.g., phosphonic acid) functionalities were blended (at 1-3 wt.%) into PAN
7 sol gels used for electrospinning, yielding functionalized nanofiber mats. For comparison, we
8 also functionalized PAN nanofibers with amidoxime (AO) moieties, a group well-recognized for
9 its specificity in U^{6+} uptake. For optimal N-based (Aliquat® 336 or Aq) and P-containing
10 [hexadecylphosphonic acid (HPDA) and bis(2-ethylhexyl)phosphate (HDEHP)] binding agents,
11 we then explored their use for U^{6+} removal across a range of pH values (pH 2-7), U^{6+}
12 concentrations (up to 10 μ M), and in flow through systems simulating point of use (POU) water
13 treatment. As expected from the use of quaternary ammonium groups in ion exchange, Aq-
14 containing materials appear to sequester U^{6+} by electrostatic interactions; while uptake by these
15 materials is limited, it is greatest at circumneutral pH where positively charged N groups bind
16 negatively charged U^{6+} complexes. In contrast, HPDA and HDEHP perform best at acidic pH
17 representative of mine drainage, where surface complexation of the uranyl cation likely drives
18 uptake. Complexation by AO exhibited the best performance across all pH values, although U^{6+}
19 uptake via surface precipitation may also occur near circumneutral pH value and at high (10 μ M)
20 dissolved U^{6+} concentrations. In simulated POU treatment studies using a dead-end filtration
21 system, we observed U removal in AO-PAN systems that is insensitive to common co-solutes in
22 groundwater (e.g., hardness and alkalinity). While more research is needed, our results suggest
23 that only 80 g (about 0.2 lbs.) of AO-PAN filter material would be needed to treat an individual's
24 water supply (contaminated at ten-times the U.S. EPA Maximum Contaminant Level for U) for
25 one year.

26

27

INTRODUCTION

28

29

30

31

32

33

34

35

36

37

38

39

40

41

42

43

44

45

46

47

48

49

Uranium (U) contamination affects the drinking water of many consumers in the Four Corners region of the United States (Colorado, New Mexico, Arizona, and Utah), including indigenous communities such as the Navajo Nation.¹ Mining of U ore deposits in the region occurred between 1940 and 1980 but left a profound impact on the environment because of the presence of thousands of abandoned and open mines.²⁻³ Over 500 abandoned mines containing residual U within waste rock are located on Navajo lands and contribute to U concentrations in unregulated water sources that exceed the U.S. Environmental Protection Agency Maximum Contaminant Limit (US EPA MCL) of 30 $\mu\text{g/L}$.⁴⁻⁷ In surface waters and shallow aquifers, U is in the hexavalent state and forms the uranyl (UO_2^{2+}) cation, which can further complex to ligands to form soluble species.⁸ Source waters in the region range from alkaline to circumneutral pH and are high in dissolved carbonate, leading to the formation of soluble uranyl complexes that can contribute to high concentrations of total U in drinking water sources.^{5, 9-10} Some waters near mine waste sites can have pH values lower than 4 due to acid mine drainage.¹¹

For resource-constrained communities without reliable access to centralized water treatment systems, point-of-use (POU) and point-of-entry (POE) technologies are an attractive option for improving drinking water quality. For example, existing US EPA-approved small system compliance technologies (SSCT) for POU treatment of U^{6+} include ion exchange (IX) and reverse osmosis (RO) technologies, while activated alumina can also remove U^{6+} but is not listed as an SSCT.¹² Although all of these approaches are capable of removing total U to levels below the US EPA MCL, these technologies can be difficult to use and maintain in underserved populations. For example, RO can involve high capital costs, requires high operating pressures with associated energy demand, and produces a concentrated waste brine that would need proper

50 disposal.¹³ In places relying on unregulated water sources,¹⁴ as is the case in some locations
 51 within the Navajo Nation,¹⁵ such advanced technologies would be of limited value.

52 We have previously demonstrated the use of electrospinning to produce novel,
 53 chemically reactive membranes for simultaneous filtration of suspended particles and
 54 sequestration or destruction of dissolved chemical contaminants.¹⁶⁻¹⁹ For materials targeting
 55 dissolved metals, we have used surface-segregating surfactants, especially those with quaternary
 56 ammonium groups, to produce surface-functionalized polymeric nanofibers that effectively
 57 function as ion exchange materials. More recently, we have also used post-fabrication routes to
 58 introduce specific binding moieties on the nanofiber surface. For U^{6+} , a popular moiety is
 59 amidoxime (AO),²⁰⁻²¹ which is highly specific for the uranyl cation and can be produced via
 60 reduction of polyacrylonitrile (PAN),²² a polymer commonly used in electrospinning, with
 61 hydroxylamine (**Table 1**). Indeed, we have previously amidoximated PAN (AO-PAN)
 62 nanofibers for the selective concentration of U^{6+} to improve environmental sensing via Surface
 63 Enhanced Raman Spectroscopy (SERS).²³ However, we have not yet explored this material more

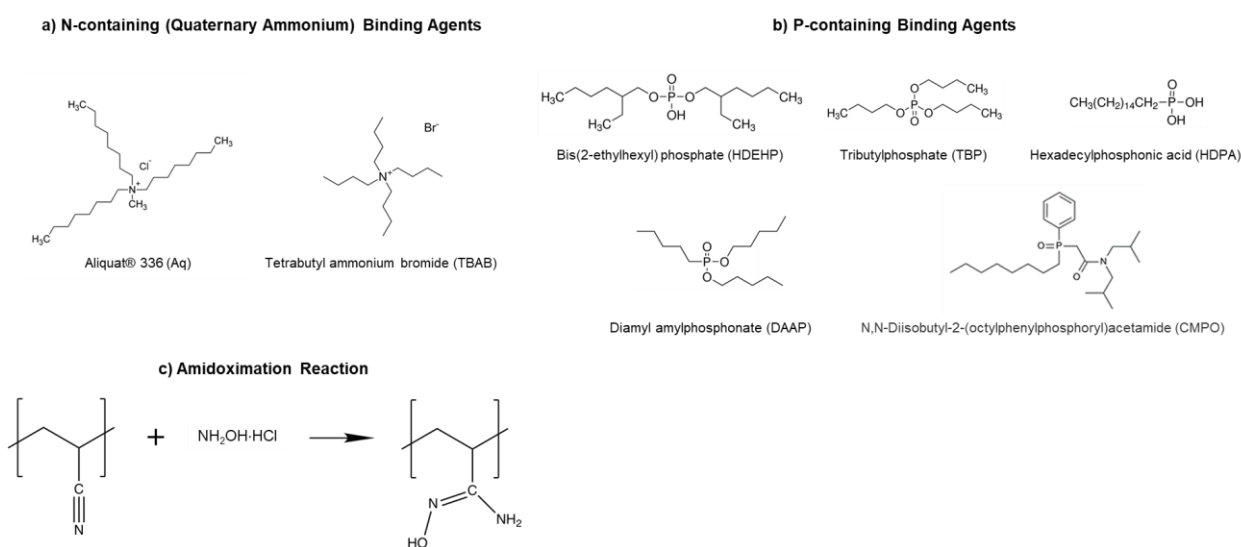


Table 1. (a) N-containing (quaternary ammonium) and (b) P-containing binding agents, as well as (c) the amidoximation reaction of PAN, used for U capture herein.

64 generally for water treatment applications, where timescales of uptake, material capacity,
65 performance across pH, and response to common co-solutes (e.g., alkalinity and hardness typical
66 of U-contaminated waters) will undoubtedly influence performance.

67 Here, we fabricate various functionalized PAN nanofibers using electrospinning and
68 explore their applications for the removal of U^{6+} from contaminated water supplies. To
69 introduce U^{6+} -specific binding sites, we not only used post-synthesis amidoximation of PAN
70 nanofibers, but we also developed synthesis recipes integrating various N- and P-containing
71 surfactants to produce functionalized nanofibers (**Table 1**). For N-containing surfactants, we
72 focused on those with quaternary ammonium groups (e.g., tetrabutyl ammonium bromide or
73 TBAB and Aliquat® 336)²⁴⁻²⁵ because these are analogous to strong-base anion exchange sites
74 and thus would be expected to electrostatically bind negatively charged U^{6+} complexes typical of
75 circumneutral pH. P-containing binding agents included surfactants with phosphoric or
76 phosphonic acid groups [e.g., di-(2-ethylhexyl)phosphoric acid (HDEHP) and
77 heptadecylphosphonic acid (HDEHP)]²⁶⁻²⁸ that form strong complexes with U^{6+} and may
78 ultimately promote more extensive removal via surface precipitation. We also explored the
79 integration of commercially available P-based extractants (diamyl amyl phosphonate (DAAP),
80 octylphenyl-N,N-diisobutylcarbamoylmethylphosphine oxide (CMPO), and tributyl phosphate
81 (TBP) that are commonly marketed (e.g., Eichrom's TRU Resin with CMPO)²⁹ to separate U^{6+}
82 from complex media in nuclear waste streams. For example, phosphate esters such as TBP have
83 been used extensively in the nuclear fuel cycle to selectively extract UO_2^{2+} cations from fission
84 products and transuranics in liquid-liquid processes; although the exact nature of this extraction
85 is not fully delineated it is suggested to proceed via outer sphere complexes, particularly with
86 uranyl nitrate species.³⁰⁻³¹

87 After nanofiber synthesis and characterization of their physical and chemical properties,
88 we tested eight different functionalized materials for U^{6+} uptake to identify the most promising
89 candidates for further material development. The performance of the most promising materials
90 for U^{6+} capture was then explored across a range of pH, dissolved U^{6+} concentrations, and water
91 chemistries, including in a dead-end, flow through filtration system typical of low-pressure POU
92 water treatment. Outcomes of this work help to establish the viability of functionalized nanofiber
93 filters as low pressure water treatment technologies for use in areas afflicted by U^{6+}
94 contamination of limited freshwater resources.

95

96

MATERIALS AND METHODS

97 **Reagents.** A complete list of reagents can be found in the Supplementary Information
98 (SI). Nanofibers of PAN (MW 150,000, Aldrich) were fabricated by electrospinning on a support
99 layer of polyvinylidene difluoride (PVDF; MW 180,000, Aldrich). Binding agents (**Table 1**)
100 included N-containing tetrabutylammonium bromide (TBAB; Sigma Aldrich) and Aliquat® 336
101 (Aq; Alfa Aesar) and P-based binding agents tributyl phosphate (TBP; Sigma Aldrich), diamyl
102 amyolphosphate (DAAP; Sigma Aldrich), CMPO (Carbosynth; 98%), bis(2-ethylhexyl
103 phosphate (HDEHP; 97%, Aldrich), and hexadecyl phosphonic acid (HDPA; 97%, Aldrich).
104 Amidoximation of PAN used hydroxylamine hydrochloride (98%, Aldrich) and sodium
105 hydroxide (97.0%, Fisher Scientific).

106 **Electrospinning.** Full details of nanofiber synthesis are provided in the SI. Nanofiber
107 mats were synthesized on a custom-built electrospinning rig described in our previous work.¹⁶⁻¹⁸
108 PAN nanofibers were deposited on a layer of PVDF nanofibers to enhance the mechanical
109 stability of the materials; PVDF was electrospun first, and after completion of the PVDF layer, a

110 layer of PAN was subsequently deposited via sequential electrospinning. The resulting bilayer
111 material contained 50 wt% PAN and 50 wt% PVDF. For production of AO-PAN, the two-layer
112 polymer structure was reacted with hydroxylamine according to the amidoximation procedure
113 described in the SI, which was adapted from our earlier work.²³

114 Mats with surfactant-based binding agents followed the same synthesis procedure but
115 used PAN sol gel precursor solutions containing the desired binding agent. Most surfactant-
116 functionalized mats were prepared using a precursor solution with 7 wt.% PAN and up to 3 wt.%
117 of binding agent dissolved in DMF (all wt.% are reported relative to the total weight of sol gel).
118 Because HDPa exhibited limited solubility in DMF, mats containing HDPa were only prepared
119 with 6 wt.% PAN and either 0.5 or 1 wt.% HDPa dissolved in DMSO. All solutions were then
120 stirred at 60°C for 2 h at 700 RPM to ensure complete dissolution of the surfactants and a
121 homogenous precursor solution.

122 **Nanofiber Characterization.** Nanofiber morphology and diameter were determined
123 through imaging with Scanning Electron Microscopy (SEM; S-4800, Hitachi). Fourier
124 Transform Infrared Spectroscopy (FTIR; Nicolet™ iS™ 50 FTIR Spectrometer) was used to
125 examine all functionalized nanofiber formulations to confirm the presence of PAN and the
126 binding agent. Mat pore volume and specific surface area were determined by N₂-BET
127 adsorption isotherms on a Quantachrome NOVA 4200e Analyzer. X-ray photoelectron
128 spectroscopy (XPS) was performed using a Kratos Axis Ultra spectrometer to characterize the
129 near surface region (~top 5-10 nm) of the functionalized nanofibers before and after U⁶⁺ uptake
130 experiments. Additional materials characterization details can be found in the SI.

131 **Uranium Uptake Experiments.** *Initial comparison of different binding agents.* To
132 identify the most promising binding agents, uptake experiments with functionalized nanofibers

133 were conducted with 10 μM total U^{6+} at either pH 2 (Milli-Q Ultrapure water adjusted with 5 N
134 HNO_3) or pH 6.8 (10 mM HEPES, which is commonly used in environmental and biological
135 systems, including our prior work with U^{6+} uptake and sensing on AO-PAN).²³ These pH values
136 were chosen for their relevance to U^{6+} treatment systems, simulating remediation of U-
137 contaminated acid mine drainage (pH 2) and treatment of U-contaminated drinking water sources
138 (pH 6.8). Solutions of U^{6+} were prepared by diluting a 1000 mg/L depleted uranium nitrate
139 (SPEX CertiPrep) stock to the desired initial concentration, typically 1 or 10 μM (0.24 or 2.4
140 ppm, or mg/L, as U^{6+} respectively), in a 50 mL plastic conical vials. To initiate an uptake study,
141 a functionalized PAN mat was added to a conical vial at a mass loading of 0.25 g/L (~ 0.25
142 cm^2/L) and then incubated while mixing. Rate experiments confirmed that uptake of U was
143 relatively rapid in all systems (see **Figure S1**), with most uptake achieved in the initial 2 h.
144 Because a small amount of U^{6+} uptake continued over longer timescales in some systems, all
145 sorption studies were allowed to proceed for 16 h, at which point there was no significant change
146 in solution concentration over time for any system (i.e., equilibrium). In all instances, minimal
147 pH drift was observed (<0.1 pH units) during the 16-hour reaction period, after which mats were
148 removed from the solution and analyzed for their sorbed U^{6+} content as described below.

149 *pH edge and isotherm experiments.* For the most promising materials identified from
150 initial uptake studies, more in depth pH-edge and isotherm experiments were conducted using
151 experimental systems identical to those described above. For pH edge experiments, systems were
152 assembled at initial pH values between 2 and 7. To avoid any influence of different buffers at
153 different pH values, all experiments were conducted in Milli-Q Ultrapure water that was adjusted
154 to the desired pH with either 5 M NaOH or HNO_3 . pH edge experiments were conducted at
155 initial U^{6+} concentrations of both 1 and 10 μM , and all systems were allowed to react for 16

156 hours to achieve equilibrium. At the conclusion of the experiment, the final pH value of each
157 reactor was recorded to measure pH drift during incubation, which was typically <0.5 pH units.

158 For sorption isotherms, initial U^{6+} solutions were prepared at concentrations of 0.1, 0.5,
159 1, 5 and 10 μM U. Sorption isotherms were conducted at either pH 2 (Milli-Q Ultrapure water
160 adjusted with either 5 N NaOH or 5 N HNO_3) or pH 6.8 (10 mM HEPES). All other
161 experimental conditions are as described previously for pH edge systems (e.g., 16 h incubation
162 period).

163 *Simulated POU filtration.* The performance of optimal nanofiber mat formulations was
164 evaluated in a dead-end, flow-through filtration system (**Figure S2**) to simulate their application
165 in water treatment. The filter holder (Cole-Parmer) had a 25 mm outer diameter with an active
166 filtration area of 3 cm^2 . Mats were cut to fit within this holder and typically weighed between 10-
167 13 mg per layer of mat (depending on the formulation). To increase the mass of nanofibers used
168 for treatment, thicker filters were created by stacking multiple layers of material with the same
169 effective filtration area, thereby increasing the residence time for U-containing influent within
170 the nanofiber mat. Flow-through conditions were created using influent flowrates of 0.4 or 0.8
171 mL/min driven by a 60 mL syringe loaded on a syringe pump (New Era Pump Systems, Inc.).
172 These flowrates correspond to fluxes ranging from 80 to 160 LMH (0.4 to 0.8 mL/min assuming
173 3 cm^2 active area), which correspond to the high range for ultrafiltration (80 LMH) and low end
174 of microfiltration (160 LMH).³² Filters were pre-conditioned with 20 mL of a 10 mM HEPES
175 solution (pH 6.8) followed by either 120 or 240 mL of a 1 μM U^{6+} (0.24 ppm) solution in 10 mM
176 HEPES at pH 6.8. Additional tests were conducted using solutions with 500 mg/L Ca^{2+} and 500
177 mg/L HCO_3^- to evaluate the influence of environmentally relevant ions. Effluent was collected

178 in 4 mL samples for every 10 mL of filtered solution for analysis of dissolved U by ICP-MS as
179 described below.

180 **Analytical Methods.** For batch uptake systems, U analysis was conducted via liquid
181 scintillation counting (LSC) using a ^{232}U radiotracer (NIST traceable standard, Eckert & Ziegler)
182 with a 3.5 Bq spike per 20 mL of solution. The activity of solutions was measured by adding 2
183 mL aliquots from each reactor to 10 mL of EcoLite scintillation cocktail (MP Biomedicals) in a
184 20 mL scintillation vial. Sorbed uranium was measured by removing the mat from the reactor
185 and placing it into a 20 mL scintillation vial with 10 mL of Ecolite scintillation cocktail. Vials
186 were shaken and left overnight to dark adapt (energy in scintillation cocktail from light is able to
187 leave) and provide ample time for the polymer mats to dissolve in the scintillation cocktail.
188 Samples were then counted on a liquid scintillation counter (LSC; Packard 1600CA Tri-Carb
189 Liquid Scintillation Analyzer) for 40 minutes. The range of 100 and 2000 keV was used to
190 exclude beta signals produced by daughter isotopes of ^{238}U , ^{234}Th and ^{234}Pa . Generally, in
191 samples collected from equilibrated experimental systems, LSC analysis of both solution phase
192 and sorbed uranium indicated complete mass balance.

193 ICP-MS analysis was used to analyze the effluent for U^{6+} collected from the flow through
194 systems. Effluent samples analyzed by ICP-MS analysis were acidified with 2% HNO_3 (trace
195 metals grade, Aldrich) and filtered with 0.45 μm filters prior to analysis on an Agilent
196 Technologies 7900 ICP-MS. Argon was used as the carrier gas in low matrix mode and no
197 collision gas was used. Mass-to-charge ratios of 7, 89, and 205 were used for tuning of the
198 instrument prior to running calibration standards and samples in triplicate. ^{209}Bi (Inorganic
199 Ventures) was used as the internal standard at a concentration of 10 ppb. We note, initial studies
200 indicated that trace amounts of some surfactants likely leached from the functionalized mats

201 during uptake experiments, and this dissolved surfactant residual present in samples interfered
202 with ICP-MS analysis. To avoid this interference, all surfactant-functionalized materials were
203 washed with DI water prior to use in uptake experiments where samples required ICP-MS
204 analysis (e.g., flow through systems). The washing procedure involved placing 5 mg of a
205 functionalized PAN mat in a 50 mL conical vial with 10 mL of Milli-Q Ultrapure water. Vials
206 were mixed end over end for 24 hours, while three changes of the water were performed over
207 that time interval.

208

209 RESULTS AND DISCUSSION

210 **Comparison of Functionalized PAN Nanofibers for U^{6+} Uptake.** Initial uptake studies
211 explored the performance of PAN nanofibers functionalized with different P- and N-containing
212 binding agents as a function of their wt.% in PAN at pH 2 and pH 6.8 (**Figure 1**). Of the P-
213 functionalized materials, integration of HDEHP (at pH 2) and HDPA (at pH 2 and 6.8) resulted
214 in the greatest uptake (between 35-55% uptake for 0.25 g/L of nanofibers and initially 10 μ M
215 U^{6+}), with U^{6+} binding on other P-containing materials (e.g., TBP, CMPO, and DAAP) being
216 very limited (~10%) or negligible at both pH values. Performance of HDEHP was effectively
217 invariant over the concentrations in PAN we explored (1 and 3 wt.%); thus, all additional work
218 with HDEHP was conducted at 1 wt.% to minimize the amount of reagent needed for synthesis.
219 For HDPA-containing materials, optimal performance was observed at a concentration of 0.5
220 wt.% in PAN.

221 For N-containing binding agents, U^{6+} uptake was only observed at pH 6.8, with no
222 detectable binding at pH 2. Generally, Aq-containing materials outperformed those with TBAB.
223 Although comparable uptake of U was observed for 1 wt.% in PAN of either Aq or TBAB,

224 increasing the concentration to 2 wt.% resulted in higher uptake with Aq but lower uptake for
 225 TBAB-containing materials. We have previously found that the mass ratio of quaternary
 226 ammonium surfactant to polymer can influence the performance of the functionalized PAN.¹⁷
 227 Accordingly, additional studies exploring the influence of Aq concentration between 0.5 to 4
 228 wt.% were conducted, revealing maximum U⁶⁺ uptake at 2 wt% in PAN. All additional uptake
 229 studies were conducted at this optimal Aq loading.

230 AO-PAN exhibited the greatest uptake at pH 6.8, nearly double of the removal displayed
 231 by either HDPA- or Aq-containing materials at the same pH value. At pH 2, AO-PAN also

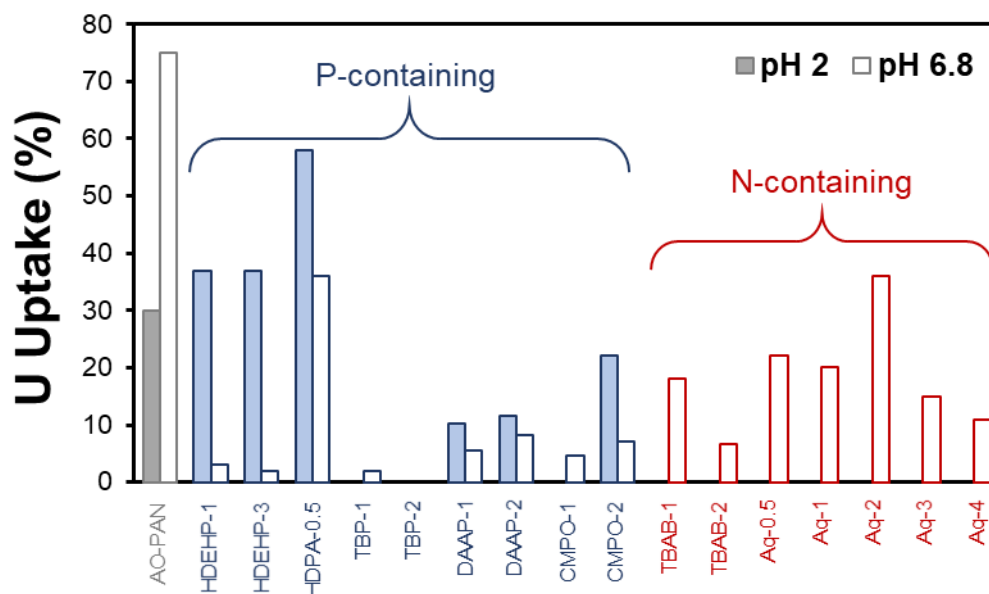


Figure 1. Performance comparison of functionalized PAN nanofibers for U⁶⁺ uptake at pH 2 (solid bars) and pH 6.8 (open bars). Uptake data are shown for different binding agents (with wt.% in sol gel indicated) after 16 h of equilibration between an initial concentration of 10 μM U⁶⁺ and 0.25 $\text{g}\cdot\text{L}^{-1}$ of each mat. Experiments were conducted in 10 mM HEPES at pH 6.8 and water acidified to pH 2 with HNO₃.

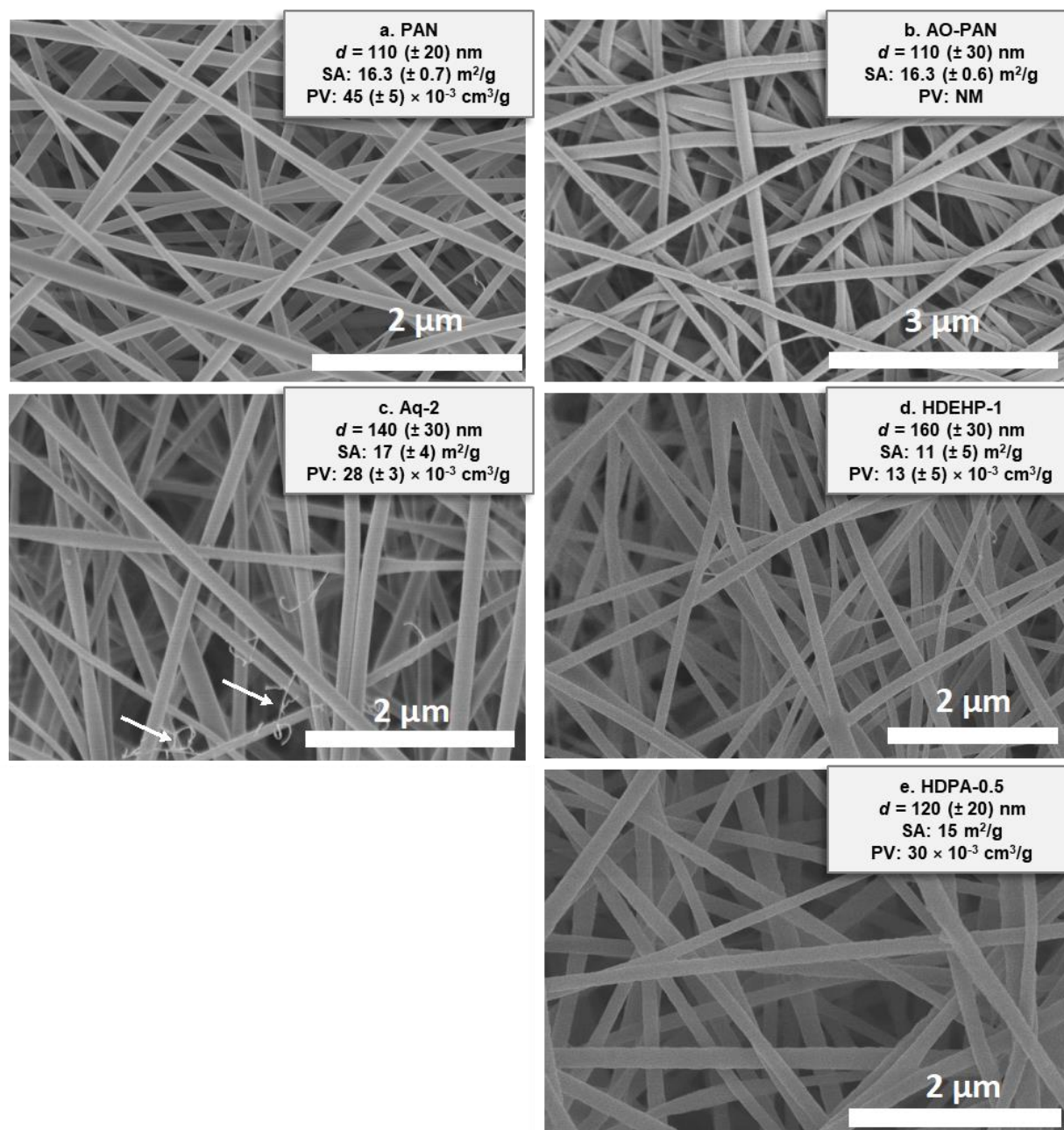


Figure 2. Representative SEM images of synthesized nanofibers, where the numbers in the material name correspond to the wt.% of the integrated surfactant (where appropriate). Also provided are results from N_2 -BET measurements of specific surface area (SA in m^2/g) and pore volume (PV in cm^3/g). Average and standard deviations are provided from duplicate measurements, where available. NM means “Not Measured”, as there was insufficient amount of material fabricated to allow for SA or PV analysis. For some surfactant-functionalized materials (e.g., Aq), small amounts of “hair-like” structures were observed (see white arrows) but were not present in sufficient abundance to alter nanofiber diameter distributions.

232 produced measurable uptake of U^{6+} at a level comparable to that observed for HDEHP-

233 containing materials but below the extent of removal achieved with HDPA-functionalized PAN.

234 We note that beyond basic characterization to ensure all materials tested in **Figure 1** were
235 comparable in morphology (i.e., nanofibers), no additional investigations were performed to
236 better understand differences in the performance of P- and N-containing binding agents. Several
237 possibilities exist, including differences in the chemistry of the binding sites available on the
238 functionalized PAN (e.g., the relative affinity for U^{6+} uptake on different P-containing
239 functionalities). We also cannot rule out differences in the location of the binding sites in the
240 fibers after electrospinning, as some binding agents may surface segregate to a greater extent
241 than others. Thus, it is certainly possible that the performance of materials with low U^{6+} uptake
242 in **Figure 1** could be further optimized, but such work is beyond the scope of the current study.

243 **Characterization of Optimally Performing Nanofibers.** Key characterization details for
244 optimal nanofiber formulations including AO-PAN and those containing either 2 wt.% Aq, 0.5
245 wt.% HDPA, or 1 wt.% HDEHP are summarized in **Figure 2**. Overall, there were only a few
246 notable differences between the functionalized PAN nanofibers explored for U uptake. The
247 average diameter for all functionalized PAN nanofibers was between 110-160 nm, but the typical
248 standard deviation from the nanofiber distribution (see histograms in **Figure S3**) indicates all
249 diameters are statistically equivalent. Moreover, there was no obvious influence of increasing
250 functionalization, either based on wt.% of embedded P- or N-containing binding agents or
251 amidoximation, on the average or distribution of nanofiber diameters. Similarly, the specific
252 surface area for all materials fell between 11 and 21 m^2/g (with most being statistically equivalent
253 based on the standard deviation from replicate analyses), with no clear trends in surface area based
254 upon the amount or type of integrated binding sites. There were some modest differences in the
255 pore volume of different materials, especially for HDEHP-containing nanofibers that exhibited

256 pore volumes [$13 (\pm 5) \times 10^{-3} \text{ cm}^3/\text{g}$] considerably lower than the other materials [for example, 45
257 $(\pm 5) \times 10^{-3} \text{ cm}^3/\text{g}$ for PAN]. We speculate this could be an indication that HDEHP preferentially
258 locates within the pore structure of PAN, blocking pore access. Analysis via FTIR (**Figure S4**)
259 was consistent with expectations for PAN-based polymers, but typically revealed little evidence
260 of the different functionalization routes we employed except for HDEHP and amidoximation. This
261 is not necessarily surprising because FTIR is a bulk characterization technique and most binding
262 agents were present at a relatively low wt.% in the functionalized nanofibers.

263 **pH-Dependent U Uptake.** At an initial U^{6+} concentration of $10 \mu\text{M}$, PAN with 0.5 wt.%
264 HDPA exhibited among the highest uptake ($>60\%$ of total U^{6+}) over the entire pH range (**Figure**
265 **3a**). AO-PAN achieved its lowest removal at pH 2 ($\sim 40\%$), but U^{6+} removal increased with pH,
266 producing relatively high and constant removal between pH 3 and 7 ($\sim 80\%$). PAN with 1 wt.%
267 HDEHP exhibited the opposite behavior relative to AO-PAN; its highest uptake was at pH 2
268 ($\sim 50\%$), but U^{6+} removal decreased markedly at pH 3 ($< 20\%$) and was maintained at this low
269 level for all higher pH values explored. Finally, PAN with 2 wt.% Aq exhibited the lowest removal
270 overall (between 0-15%), but U^{6+} uptake did modestly increase with increasing pH values.

271 Notably, at a lower initial U^{6+} concentration of $1 \mu\text{M}$ (**Figure 3b**), different pH-dependent
272 removal trends were observed for some, but not all, materials. While trends in U^{6+} uptake at $1 \mu\text{M}$
273 were comparable to those observed at higher initial U^{6+} for HDEHP- and Aq-containing PAN,
274 AO-PAN and HDPA-containing PAN exhibited different pH-dependent performance. For AO-
275 PAN, this difference was only observed at higher pH values (pH >5). Specifically, whereas
276 removal was relatively constant ($\sim 80\%$) above pH 5 in $10 \mu\text{M}$ U^{6+} systems, uptake decreased
277 steadily from pH 5 ($\sim 80\%$) to pH 7 ($\sim 40\%$) in $1 \mu\text{M}$ U^{6+} systems. A much greater difference in
278 performance between low and high concentration U^{6+} systems was observed with HDPA-

279 functionalized PAN. While removal at $10 \mu\text{M } \text{U}^{6+}$ was greater than 60% across all pH values, the
 280 removal in $1 \mu\text{M } \text{U}^{6+}$ systems was greatest at pH 2 ($\sim 50\% \text{U}^{6+}$) and decreased steadily until pH 4
 281 ($\sim 10\%$), above which uptake was minimal.

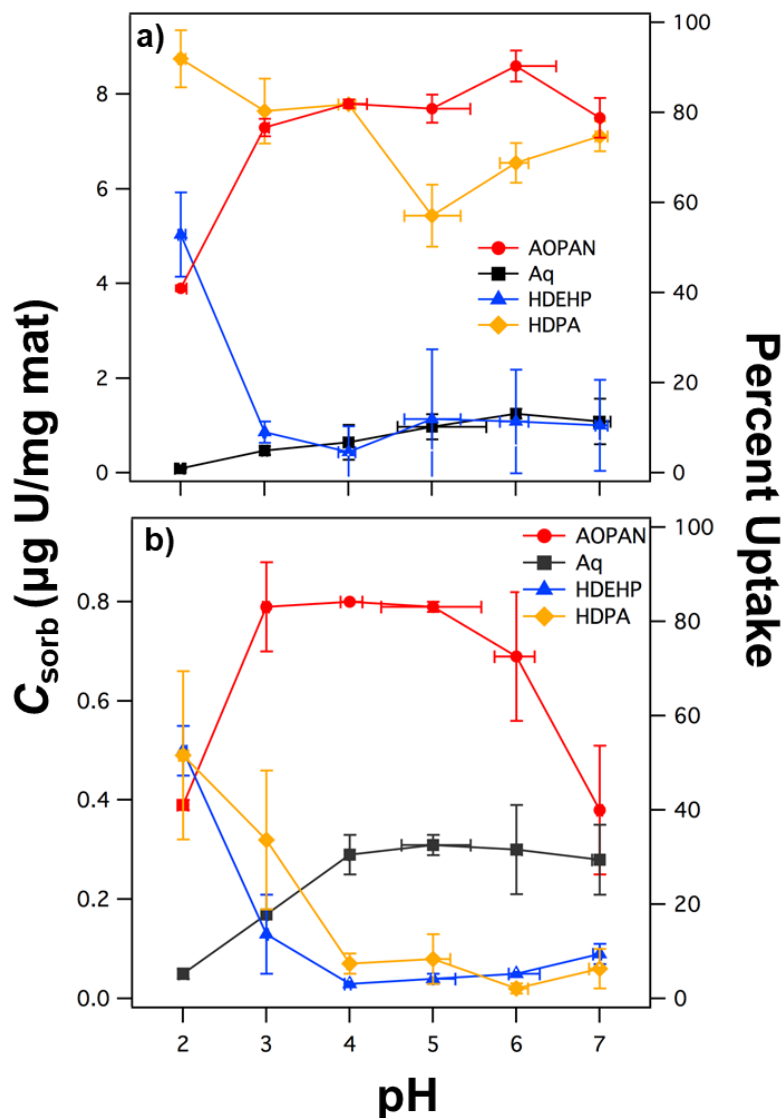


Figure 3. Sorbed U^{6+} concentration as a function of solution pH at an initial U^{6+} concentration of (a) $10 \mu\text{M}$ and (b) $1 \mu\text{M}$ for AO-PAN and PAN with either 2 wt.% Aq, 0.5 wt.% HDPA, or 1 wt.% HDEHP. All materials were tested in water (pH adjusted with 5 M NaOH or HNO_3) without buffer. Vertical error bars reflect standard deviation of duplicate trials while horizontal error bars represent the range of pH drift observed over the course of the experiment (~ 16 h). A nanofiber mass loading of 0.25 g L^{-1} was used in all experiments.

282

283 A possible explanation for the difference in performance between 1 μM and 10 μM U^{6+}
284 systems for AO-PAN and HDP-PA-containing materials could be removal via surface precipitation
285 at high initial U^{6+} concentrations, similar to processes previously reported to occur on mineral
286 phases³³ and functionalized polymers.³⁴ For AO-PAN, for example, the exact binding mechanism
287 for uranium to amidoxime is still widely disputed, with arguments for either monodentate (binding
288 with either N or O) or bidentate (binding to both N and O) complexes in prior investigations.³⁵
289 Pekel et al.³⁶ suggested that deprotonation of the imine group was important for chelation to uranyl
290 by exchange of H^+ with UO_2^{2+} while Hirotsu et al.³⁷ reported that ligand exchange (and ion
291 exchange of H^+ depending on pH) occurs during uranyl uptake. In both 1 and 10 μM U systems at
292 pH 2, similar uranium removal occurs ($\sim 40\%$) with 100% of the uranyl species being UO_2^{2+} ,
293 suggesting that the high H^+ concentration competes with UO_2^{2+} in the amidoxime group. A
294 decrease in the H^+ concentration (i.e., increasing pH between 3 and 5) results in much greater
295 ($\sim 80\%$) U^{6+} removal. Hydrolysis of UO_2^{2+} starts at pH 4, and it is no longer the dominant species
296 by pH 5 (see Guillaumont et al.³⁸ and speciation diagrams for 1 and 10 μM U^{6+} solutions in **Figure**
297 **S5**). In 10 μM systems, speciation diagrams suggest that insoluble $\text{UO}_2(\text{OH})_2 \cdot \text{H}_2\text{O}$ is the dominant
298 species by pH ~ 5.5 , and we suspect this species may be precipitating on the surface based upon
299 the high ($\sim 80\%$) removal still observed at pH 6 and 7 in 10 μM U^{6+} systems. In contrast, the
300 decrease in removal with increasing pH observed in 1 μM U^{6+} systems ($\sim 70\%$ at pH 6 and $\sim 40\%$
301 at pH 7) may be indicative of speciation changes that occur above pH 5; we expect UO_2OH^+ to be
302 the dominant form at pH 5 and 6 ($\sim 50\%$ and $\sim 40\%$ of total U^{6+} , respectively) followed by
303 $\text{UO}_2(\text{OH})_2 \cdot \text{H}_2\text{O}$ at pH 7 ($\sim 90\%$ of total U). Because ligand exchange is expected to occur in these
304 regions, the lower uptake may also be due to slower kinetics involved with ligand exchange.³⁹

305 For HDPA-functionalized PAN, uranyl phosphate complexes are known to have very low
306 $\log K_{sp}$ values (-49.00 to -53.33)⁴⁰ compared to that of hexavalent uranyl hydroxides (-21.75 to -
307 24.10)⁴¹ and uranyl carbonates (-13.29 to -14.91),⁴⁰ which enables uranium phosphates to
308 precipitate in even acidic solutions. This behavior has been seen before with phosphate-
309 functionalized TiO₂, where an insoluble sodium autunite (NaUO₂PO₄) complex formed after
310 uranium sorption in acidic solutions (pH 2).⁴² In this earlier work, the mechanism of uptake was
311 described as a combination of adsorption and surface complexation that shifts to surface
312 precipitation;⁴² such a scenario may also be likely for U⁶⁺ removal on HDPA-functionalized
313 nanofibers in our 10 μM U⁶⁺ systems, whereas only adsorption and surface complexation occur in
314 our 1 μM U⁶⁺ systems.

315 For HDEHP- and Aq-containing nanofibers, trends in pH-dependent removal lend insight
316 into their mechanism of U⁶⁺ binding. For example, the sorption capacity of HDEHP-containing
317 materials is reduced considerably above pH 3. HDEHP has a pK_a of 1.47,⁴³ and thus will become
318 increasingly more deprotonated (i.e., more anionic) from pH 2 to pH 3. Over this same pH range,
319 U⁶⁺ removal decreases from 50% to ~10% in both 1 and 10 μM systems. Thus, U⁶⁺ removal does
320 not appear to proceed via a purely electrostatic mechanism (i.e., positively charged UO₂²⁺ bound
321 by negatively charged HDEHP sites), suggesting that U⁶⁺ uptake may also occur by exchange of
322 H⁺ during uranyl coordination, which has been previously observed by Kiwan and Amin.⁴⁴
323 Moreover, hydrolysis of the UO₂²⁺ cation should not affect U⁶⁺ uptake with HDEHP because
324 hydrolysis products are not abundant until pH 4 for solutions containing 1 or 10 μM U⁶⁺ (see
325 Guillaumont et al.³⁸ and **Figure S5**). As a final consideration, the chemical differences between
326 HDEHP and HDPA may also lend insight regarding the mechanism of U⁶⁺ uptake. HDEHP
327 contains only one hydroxyl group available for U⁶⁺ binding, whereas HDPA has multiple

328 hydroxyls that may allow it to chelate and precipitate U^{6+} in a manner similar to the phosphate
329 anion.

330 At both initial concentrations (1 and 10 μ M), Aq-containing nanofibers produced a slight
331 increase in U^{6+} uptake with increasing pH. This behavior likely reflects that uptake of U^{6+} by Aq
332 is dependent on the fraction of anionic uranyl species present in solution. Aq is positively charged
333 across the pH range investigated, and as a strong base ion exchanger, it has been shown to bind
334 negatively charged uranium complexes.⁴⁵⁻⁴⁷ We therefore hypothesize that anion exchange is the
335 main mechanism for uptake of U^{6+} on Aq-functionalized nanofibers, but further verification of this
336 mechanism is warranted. In fact, for pure aqueous systems, anionic uranyl species (e.g. $UO_2(OH)_3^-$
337) should not be formed until \sim pH 7 (see Guillaumont et al.³⁸ and **Figure S5**). Furthermore, while
338 negatively charged species can form in the presence of carbonate [e.g., $(UO_2)_2CO_3(OH)_3^-$ can form
339 as early as pH 4], these anionic carbonate species are only produced at dissolved CO_2
340 concentrations higher than those in our experimental systems.⁴⁸

341 **Sorption Isotherms for U on Functionalized PAN Nanofibers.** To explore their capacity
342 for U^{6+} uptake, sorption isotherms were collected with AO-PAN and PAN containing either 2 wt.%
343 Aq, 0.5 wt.% HDPA, or 1 wt.% HDEHP (**Figure 4**). Functionalized PAN nanofibers were tested
344 over a range of U^{6+} concentrations that varied from just below its MCL in drinking water (\sim 0.1
345 μ M) to the more extreme levels of U^{6+} contamination that may be present in some affected water
346 resources (10 μ M). We only developed isotherms at the optimal pH value observed for each
347 functionalized material in pH-edge experiments. PAN nanofibers functionalized with HDPA and

348 HDEHP were tested in acidic conditions (pH 2), whereas isotherms for Aq-containing PAN and
 349 AO-PAN were conducted at pH 6.8.

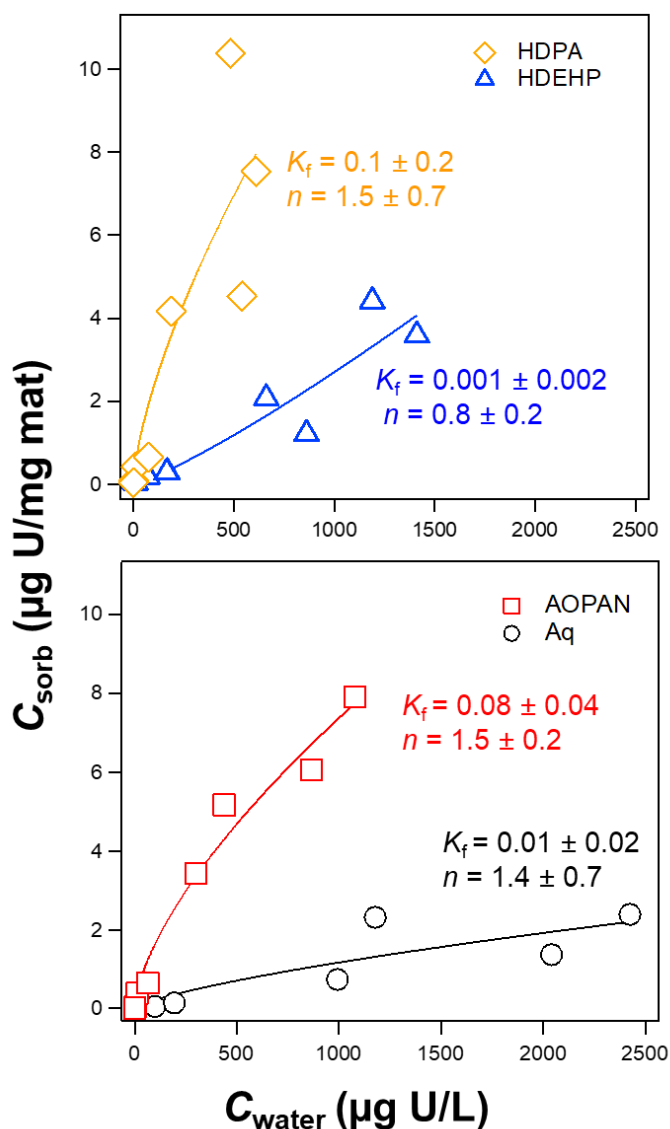


Figure 4. Sorbed U^{6+} concentration as a function of solution phase U^{6+} concentration at equilibrium for AO-PAN and PAN with either 2 wt.% Aq, 0.5 wt.% HDPA, or 1 wt.% HDEHP. Sorption isotherms were conducted in either (a) water acidified to pH 2 with HNO_3 for HDPA- and HDEHP-containing PAN or (b) 10 mM HEPES at pH 6.8 for Aq-containing and AO-functionalized PAN. Freundlich equation fits with model fit parameters are shown. Data are shown from duplicate isotherm experiments conducted on separate days with each material.

350

351 Overall, a trend of increasing solution phase U^{6+} concentration resulted in increased sorbed
352 U^{6+} concentrations for all materials, and the extent of uptake generally agreed well with our other
353 experimental results (see Figures 1 and 3). To model U^{6+} uptake, we used the empirical Freundlich
354 isotherm model [$C_{\text{sorbed}} = K_f \cdot (C_{\text{aq}})^{1/n}$, where K_f is the Freundlich isotherm parameter and n is the
355 degree of linearity] because we observed no clear evidence consistent with surface site saturation
356 (as would be expected for a Langmuir-type isotherm). The parameters for the Freundlich isotherms
357 determined by non-linear regression analysis are summarized in **Figure 4** for each functionalized
358 material. At pH 6.8, AO-PAN far exceeded the uptake of Aq-containing mats, and uptake on AO-
359 PAN was clearly non-linear ($n = 1.5 \pm 0.2$). At pH 2, U^{6+} sorption on HDPA-functionalized PAN
360 ($n = 1.5 \pm 0.7$) was considerably greater than HDEHP-containing materials ($n = 0.8 \pm 0.2$), with
361 model outputs indicating that sorption isotherms did not significantly differ from linearity over the
362 range of U^{6+} concentrations explored (although relatively large standard deviations in model fits
363 were observed because of the modest degree of variability in uptake observed between two
364 replicate isotherm experiments).

365 Even when uptake was clearly non-linear (e.g., AO-PAN), we did not achieve the sorption
366 capacity of any materials using these isotherm conditions. At the highest initial U^{6+} concentration
367 explored of 10 μM (or 2.4 mg/L), corresponding concentrations for sorbed U^{6+} were approximately
368 4 and 10 $\mu\text{g}/\text{mg}$ at pH 2 for HDEHP- and HDPA-containing nanofibers, respectively, and
369 approximately 2 and 8 $\mu\text{g}/\text{mg}$ at pH 6.8 for Aq-containing and AO-PAN nanofibers, respectively.
370 A prior investigation of AO-PAN nanofibers with a polystyrene core shell reported a maximum
371 sorbed concentration of 130 $\mu\text{g}/\text{mg}$ (conditions: 1 g mat L^{-1} ; initial uranium concentration of 100
372 mg/L; pH 4).⁴⁹ Phosphate-functionalized polyethylene had a maximum sorbed concentration of
373 180 $\mu\text{g}/\text{mg}$ (conditions: 0.2 g mat L^{-1} ; initial uranium concentration of 50 mg/L; pH 8.2).⁵⁰ Strong

374 base anion exchangers, similar to Aq, have not been used for U^{6+} uptake in nanofibers but show
375 high uptake in resins at $\sim 50 \mu\text{g}/\text{mg}$ in groundwater (conditions: initial U^{6+} concentration of 1,200
376 $\mu\text{g}/\text{L}$; pH 6.5; flow through system).⁴⁵ Although many of these prior investigations report sorbed
377 U^{6+} concentrations that are greater than what we report for the functionalized nanofibers herein,
378 we note that several of these earlier works used initial U^{6+} levels far exceeding the concentrations
379 used in our experimental systems. Thus, we cannot rule out that some of these high levels of U^{6+}
380 uptake may reflect U^{6+} removal via surface precipitation, as we suspect may occur at high U^{6+} and
381 high pH on AO-PAN and HDPA-functionalized PAN, leading to greater removal via multi-layer
382 growth of a separate U-containing solid phase.

383 To probe the nature of surface bound U^{6+} , XPS analyses were collected for all
384 functionalized materials after U^{6+} uptake experiments conducted with an initial concentration of
385 10 μM . XPS analysis of these reacted nanofiber mats detected the presence of U^{6+} on the surface
386 of all functionalized materials (**Table S1**). High resolution U 4f spectra (**Figure S6**) contained
387 signals corresponding to the U 4f_{7/2} and U 4f_{5/2} doublet on HDPA-, HDEHP-, Aq- and AO-PAN
388 functionalized materials. However, while confirming the presence of U^{6+} on the surface of all
389 functionalized nanofibers, XPS analysis was unable to provide any greater details regarding the
390 nature of U^{6+} surface species or complexes.

391 **Simulated Treatment in Flow Through Systems.** Break through curves showing
392 normalized U^{6+} concentration (i.e., effluent concentration normalized to influent concentration;
393 $C_{\text{effluent}}/C_{\text{influent}}$) as a function of volume of water treated from dead-end filtration flow through
394 systems are shown in **Figure 5** for AO-PAN and HDPA-containing nanofiber filters at pH 6.8.
395 For such curves, we define filter exhaustion or complete breakthrough as when the effluent U^{6+}
396 concentration is equal to that of the influent concentration ($C_{\text{effluent}} = C_{\text{influent}}$), which would mean

397 either that the materials are saturated (i.e., all binding sites are occupied and thus not capable of
398 removing any more uranium) or that timescales for U^{6+} uptake on the remaining available binding
399 sites are far slower than the residence time for U^{6+} in the nanofiber filter system. With an influent
400 concentration of $1 \mu M U^{6+}$ ($240 \mu g/L$) at pH 6.8, we note that any normalized concentration above
401 ~ 0.1 would be considered above the MCL for uranium ($30 \mu g/L$).

402 For AO-PAN (**Figure 5a**), the lowest filter mass tested (13 mg) did not show complete
403 breakthrough, but produced approximately constant, incomplete ($\sim 40\%$) removal of U^{6+} where
404 C_{effluent} was $\sim 60\%$ of C_{influent} . Increasing the mass of AO-PAN (from 13 mg to 26 mg by adding a
405 second filter layer) resulted in effectively complete removal of U^{6+} . Based on these results, U^{6+}
406 uptake on AO-PAN filters appears kinetically limited under our experimental conditions. At lower
407 filter mass (13 mg), breakthrough was effectively steady state; complete saturation of the filter did
408 not occur (i.e., there was always some residual capacity for U^{6+} removal), but U^{6+} was present in
409 the effluent and the effluent concentration was not changing over time. When more mass was
410 added to the filter (from 13 mg to 26 mg) then the contact time between the U^{6+} -containing solution
411 and the AO-PAN also increased, which resulted in near-complete removal of U from the 120 mL
412 sample volume. Notably, at the conclusion of the experiment with the 26 mg filter, the mass of
413 U^{6+} captured was $\sim 1.1 \mu g/mg$ after treating 120 mL of water, which is well below the maximum
414 sorbed concentration of $\sim 8 \mu g/mg$ observed in batch isotherm experiments with AO-PAN (see
415 Figure 3). This suggests that AO-PAN materials still have considerably more sites available for
416 U^{6+} binding. A second run of a 26 mg filter over 240 mL of $1 \mu M U^{6+}$ influent revealed removal
417 of all influent uranium to levels that were below detection in the effluent and thus below the EPA
418 MCL (**Figure S7**; all C_{effluent} values were below detection or $1 \mu g/L$ via our ICP-MS analytical
419 method). Once again, this sample still had not reached saturation and the amount of U^{6+} bound on

420 the reacted AO-PAN filter ($\sim 2.2 \mu\text{g}/\text{mg}$) was only $\sim 25\%$ of the max U^{6+} sorption found in batch.

421 Once again, this supports kinetically limited U^{6+} removal in AO-PAN systems, where thicker filter

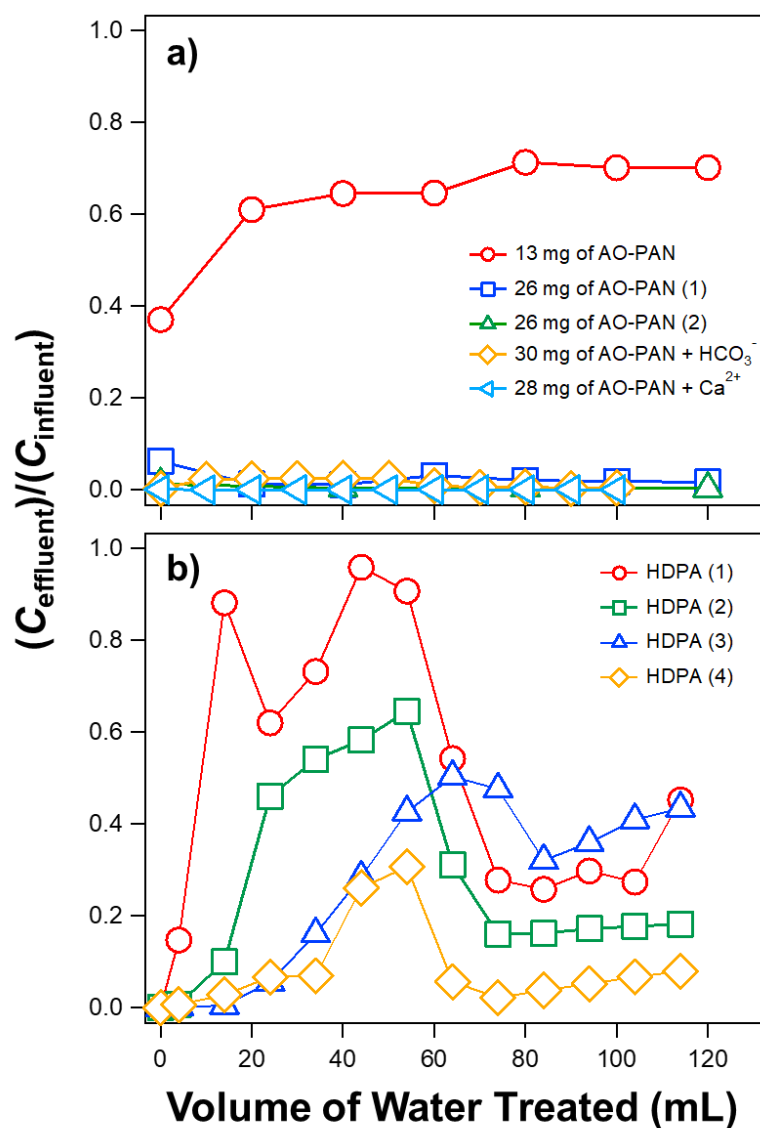


Figure 5. Normalized concentration (effluent concentration divided by influent concentration) of U^{6+} as a function of the volume treated in a dead-end filtration setup with (a) AO-PAN and (b) 0.5 wt.% HDPA-functionalized PAN. Experiments used an influent concentration of $1 \mu\text{M}$ in 10 mM HEPES (pH 6.8) and a flowrate of 0.8 mL/min (160 LMH), unless otherwise indicated. For AO-PAN, results are shown for different masses (thicknesses) of filters (13 and 26 mg), replicate filters (1 and 2) and more complex solution chemistries (500 mg/L of Ca^{2+} or HCO_3^- adjusted to pH 6.8). For HDPA-functionalized materials, four replicate experiments (1 through 4) with 20 mg filters are shown.

422 materials or lower flow rates will produce higher residence times and better removal performance.

423

424 For AO-PAN filters, the presence of Ca^{2+} (as a competing ion to simulate hardness) and
425 CO_3^{2-} (as a ligand for uranyl from alkalinity) had no influence on U^{6+} removal (**Figure 5a**). Using
426 higher mass filters (26 mg), there was no detectable U^{6+} in the filter effluent across 120 mL of
427 treated volume for either influent solution. Sorbed uranium from the Ca^{2+} and CO_3^{2-} runs were
428 nearly identical to the experiments performed in the absence of competing ions, with U^{6+} contents
429 of $\sim 1.2 \mu\text{g}/\text{mg}$ for all three trials (as determined by LSC analysis of the reacted filter). The lack of
430 interference from Ca^{2+} and CO_3^{2-} may be due to the chemical complexation of U^{6+} by AO groups
431 on the surface of the mats as opposed to electrostatic interactions that could potentially be impacted
432 by co-solute ions. It should also be noted that the pH of the solution varied from 6.8 to 7.5 over
433 the course of experiments containing the CO_3^{2-} anion, suggesting that some HCO_3^- may have been
434 scavenged by AO-PAN during the run by either amidoxime or residual nitrile groups.

435 Different behavior was observed in flow through experiments performed with the HDPA-
436 functionalized filters. Results from four replicate experiments are shown in **Figure 5b**. Partial
437 U^{6+} removal was observed with each HDPA-containing filter, with detectable U^{6+} in most effluent
438 samples across the four replicate studies. The degree of U^{6+} removal was also highly variable from
439 one experiment to the next, with some systems routinely achieving more than 80% removal of
440 influent U^{6+} (at $1 \mu\text{M}$), while much less removal and more rapid breakthrough was observed in
441 other instances. Another noteworthy feature observed in all systems was a period of increasing
442 U^{6+} removal after an initial period of more rapid breakthrough, observed by the clear localized
443 maxima in $C_{\text{effluent}}/C_{\text{influent}}$ values in each of the four replicate experiments (see maxima after 40-
444 80 mL of treated influent in **Figure 5b**).

445 We propose that these unique U breakthrough profiles result from the mechanism of
446 surface binding responsible for U^{6+} removal in HDPA-filter systems. From pH edge experiments

447 at elevated U^{6+} concentration (10 μM), surface precipitation likely contributes to U^{6+} removal at
448 near-neutral pH values. In contrast, from pH edge experiments at lower initial U^{6+} concentrations
449 (1 μM), more limited removal was observed by HPDA-containing nanofibers at near-neutral pH,
450 with any uptake presumably occurring via complexation between the phosphonic acid group on
451 HDPA and soluble U^{6+} species. By analogy, we would expect initial removal in our flow through
452 systems to occur via complexation but be relatively limited, consistent with the early periods of
453 U^{6+} breakthrough observed in filter effluent. We would also expect that after some period of filter
454 exposure to influent U^{6+} enough U^{6+} would be bound on the HDPA-functionalized surface to
455 initiate formation of higher order U^{6+} species (e.g., dimers, trimers, oligomers and eventually a
456 separate surface phase). If the rate of formation of these higher order species (resulting from
457 surface bound U^{6+} interacting with dissolved U^{6+} species) is faster than the rate at which available
458 HDPA sites form new surface complexes with dissolved U^{6+} species, we would anticipate the
459 extent of U^{6+} removal in our filter systems to increase over time.

460 Such a biphasic mechanism for U^{6+} removal (i.e., first HDPA complexing U^{6+} followed by
461 formation of higher order U^{6+} species through bound U-soluble U interactions) would likely
462 explain the high variability observed in break through curves for HDPA-containing filters in
463 **Figure 5b**. A critical point in the break through curve will be when formation of higher order
464 surface U^{6+} species begins, and it is likely the occurrence of such a transition point would be
465 dependent on highly localized factors related to the flow path through the nanofiber filter. For
466 example, if we consider the amount of U^{6+} mass accumulated in the filter over time (**Figure S8**),
467 a clear increase in the rate of U^{6+} removal is observed between 40-60 mL of treated influent for all
468 replicates, at which we suspect the transition from U^{6+} -complexation by HDPA to formation of
469 higher order U^{6+} surface species occurs. Notably, however, in all cases, the surface U^{6+}

470 concentration is relatively low (on the order of 1.2 $\mu\text{g}/\text{mg}$ mat or less; see Figure S8). Indeed,
471 because of the relatively low loading of surface U^{6+} , far less than observed for U-containing
472 samples previously characterized spectroscopically (see Figure S5), we were unable to detect any
473 surface U^{6+} via XPS on these reacted filters to further explore differences in bound species as a
474 function of filter run time. We are currently exploring the use of other spectroscopic methods
475 (e.g., XAFS) which may be better suited for examining the nature of bound U^{6+} in HDPA nanofiber
476 filtration systems.

477

478 ENVIRONMENTAL IMPLICATIONS

479 In this work, we have produced various functionalized nanofibers for binding of U^{6+} . Of
480 the materials we explored, the strongest performance across all system conditions was AO-PAN,
481 which has been widely used for capture of U^{6+} from various matrices. AO-PAN exhibited high U^{6+}
482 capacity and sustained performance during filtration, even in the presence of more complex
483 solution compositions (e.g., hardness and alkalinity). Based on our dead-end filtration
484 experiments, and assuming that the average person consumes 2 L of water daily, our results suggest
485 it would only require 80 g (about 0.2 lbs.) of AO-PAN filter material to treat water contaminated
486 with 1 μM U^{6+} to levels below US EPA standards and our method of detection (e.g., 1 $\mu\text{g}/\text{L}$ via
487 our ICP-MS analytical method) for one year.

488 While other materials exhibited less capacity for U^{6+} uptake, there still may be advantages
489 to these alternative formulations. From a fabrication standpoint, amidoximation requires post-
490 processing of electrospun PAN and uses highly concentrated and harsh reagents. The integration
491 of N- and P-containing surfactants directly into the electrospinning sol gel affords more simplicity
492 in filter fabrication, with less generation of chemical waste. Further, in applications of these

493 materials to sequester and concentrate U^{6+} for biomonitoring or sensing, where information about
494 solution phase speciation may be desirable, the ability to leverage different binding agents to
495 preferentially sequester separate U^{6+} species may be advantageous. For example, Aq and TBAB
496 were included herein because of the prior use of N-containing functionalities in ion exchange, and
497 thus these surfactants would be well-suited to specifically capture anionic U^{6+} species.

498 Future work is needed to better understand the nature of surface U^{6+} species on each of the
499 most promising functionalized PAN nanofibers. Herein, the levels of surface-bound U^{6+} generated
500 in our experimental systems prohibited extensive surface characterization. In particular, the
501 mechanism of U^{6+} sorption on HPDA-functionalized nanofibers merits additional investigation
502 based upon results from our flow through systems, which suggest that the surface U^{6+} species may
503 change over time with increasing total U^{6+} bound to the nanofiber surface. Characterization of the
504 bound U^{6+} species on HPDA and other functionalized nanofibers will be important to better predict
505 long-term filter performance, including the potential for inadvertent U^{6+} release during water
506 treatment applications and the potential for filter regeneration and reuse once saturation capacity
507 is achieved.

508

509 **Supplemental Information**

510 Supplemental information includes additional methodological details associated with
511 fabrication of functionalized nanofibers and U^{6+} analysis, as well as additional results related to
512 the characterization and performance of functionalized nanofibers.

513

514 **Acknowledgements**

515 Research reported in this work was supported by the National Institute of Environmental Health
516 Sciences of the National Institutes of Health under award number R01ES027145. Additional
517 support for MEC was provided through a National Research Traineeship (NRT) grant from the
518 National Science Foundation (NSF) under award number DGE-1633098 and through an NSF
519 Graduate Research Fellowship. The authors would also like to acknowledge the two anonymous
520 reviewers whose comments improved the clarity and impact of this work.

521

522 **Conflicts of Interest**

523 The authors have no conflicts of interest to declare.

524 **Literature Cited**

525

- 526 1. U.S. Environmental Protection Agency, Office of Radiation and Indoor Air, Radiation
527 Protection Division. *Technical Report on Technologically Enhanced Naturally Occurring*
528 *Radioactive Materials from Uranium Mining Volume 1: Mining and Reclamation*
529 *Background*; EPA 402-R-08-005, Washington D.C., 2008. Available at:
530 <https://www.epa.gov/sites/production/files/2015-05/documents/402-r-08-005-v1.pdf>
- 531 2. U.S. Environmental Protection Agency. *Abandoned Uranium Mines (AUM) and the*
532 *Navajo Nation: Northern Aum Region Screening Assessment Report.*; Region 9
533 Superfund Program: San Francisco, CA, 2006.
- 534 3. Moore Dias da Cunha, K.; Henderson, H.; Thomson, B. M.; Hecht, A. M., Ground water
535 contamination with 238-U, 234-U, 235-U, 226-Ra, and 210-Pb from past uranium
536 mining; cove wash Arizona. *Environ. Geochem. Health* **2013**, *36*, 477-487.
- 537 4. U.S. Government Accountability Office. *Uranium Contamination: Overall Scope, Time*
538 *Frame, and Cost Information is Needed for Contamination Cleanup on the Navajo*
539 *Reservation*; GAO-14-323, Washington, D. C., 2014.
- 540 5. Blake, J. M.; Avasarala, S.; Artyushkova, K.; Ali, A. M. S.; Brearley, A. J.; Shuey, C.;
541 Robinson, W. P.; Nez, C.; Bill, S.; Lewis, J.; Hirani, C.; Pacheco, J. S. L.; Cerrato, J. M.,
542 Elevated Concentrations of U and Co-occurring Metals in Abandoned Mine Wastes in a
543 Northeastern Arizona Native American Community. *Environ. Sci. Technol.* **2015**, *49*,
544 8506-8514.
- 545 6. U.S. Environmental Protection Agency. *National Primary Drinking Water Regulations.*;
546 EPA 816-F-09-004, Washington D.C., 2009. Available at:
547 [https://www.epa.gov/sites/production/files/2016-](https://www.epa.gov/sites/production/files/2016-06/documents/npwdr_complete_table.pdf)
548 [06/documents/npwdr_complete_table.pdf](https://www.epa.gov/sites/production/files/2016-06/documents/npwdr_complete_table.pdf).

- 549 7. Hoover, J.; Gonzales, M.; Shuey, C.; Barney, Y.; Lewis, J., Elevated Arsenic and
550 Uranium Concentrations in Unregulated Water Sources on the Navajo Nation, USA.
551 *Exposure and Health* **2017**, *9*, 113-124.
- 552 8. Murphy, W. M.; Shock, E. L., Environmental Aqueous Geochemistry of Actinides. In
553 *Uranium: Mineralogy, Geochemistry and the Environment.*, Burns, P. C.; Finch, R. J.,
554 Eds. Mineralogical Society of American: Washington, D.C., 1999; Vol. 38, pp 221-254.
- 555 9. Linhoff, B.; Longmire, P.; Rearick, M.; McQuillan, D.; Perkins, G., Water quality and
556 hydrogeochemistry of a basin and range watershed in a semi-arid region of northern New
557 Mexico. *Environ. Earth Sci.* **2016**, *75*, 13.
- 558 10. Blake, J. M.; De Vore, C. L.; Avasarala, S.; Ali, A. M.; Roldan, C.; Bowers, F.; Spilde,
559 M. N.; Artyushkova, K.; Kirk, M. F.; Peterson, E.; Rodriguez-Freire, L.; Cerrato, J. M.,
560 Uranium mobility and accumulation along the Rio Paguete, Jackpile Mine in Laguna
561 Pueblo, NM. *Environ. Sci. Proc. Impacts* **2017**, *19*, 605-621.
- 562 11. Blake, J. M.; Avasarala, S.; Ali, A.-M. S.; Spilde, M.; Lezama-Pacheco, J. S.; Latta, D.;
563 Artyushkova, K.; Ilgen, A. G.; Shuey, C.; Nez, C.; Cerrato, J. M., Reactivity of As and U
564 co-occurring in Mine Wastes in northeastern Arizona. *Chemical Geology* **2019**, *522*, 26-
565 37.
- 566 12. U.S. Environmental Protection Agency, office of Water. *Point-of-Use or Point-of-Entry*
567 *Treatment Options for Small Drinking Water Systems*; EPA 815-R-06-010; Washington,
568 D.C., 2006.
- 569 13. Greenlee, L. F.; Lawler, D. F.; Freeman, B. D.; Marrot, B.; Moulin, P., Reverse osmosis
570 desalination: Water sources, technology, and today's challenges. *Water Research* **2009**,
571 *43*, 2317-2348.
- 572 14. Deitz, S.; Meehan, K., Plumbing Poverty: Mapping Hot Spots of Racial and Geographic
573 Inequality in U.S. Household Water Insecurity. *Annals of the American Association of*
574 *Geographers* **2019**, *109*, 1092-1109.
- 575 15. U.S. Environmental Protection Agency. *Providing Safe Drinking Water in Areas with*
576 *Abandoned Uranium Mines. Navajo Nation: Cleaning Up Abandoned Uranium Mines.*
577 Available at: [https://www.epa.gov/navajo-nation-uranium-cleanup/providing-safe-](https://www.epa.gov/navajo-nation-uranium-cleanup/providing-safe-drinking-water-areas-abandoned-uranium-mines)
578 [drinking-water-areas-abandoned-uranium-mines](https://www.epa.gov/navajo-nation-uranium-cleanup/providing-safe-drinking-water-areas-abandoned-uranium-mines) (accessed September 8, 2019).
- 579 16. Greenstein, K. E.; Myung, N. V.; Parkin, G. F.; Cwiertny, D. M., Performance
580 comparison of hematite ($\alpha\text{-Fe}_2\text{O}_3$)-polymer composite and core-shell nanofibers as point-
581 of-use filtration platforms for metal sequestration. *Water Research* **2019**, *148*, 492-503.
- 582 17. Peter, K. T.; Johns, A. J.; Myung, N. V.; Cwiertny, D. M., Functionalized polymer-iron
583 oxide hybrid nanofibers: Electrospun filtration devices for metal oxyanion removal.
584 *Water Research* **2017**, *117*, 207-217.
- 585 18. Peter, K. T.; Myung, N. V.; Cwiertny, D. M., Surfactant-assisted fabrication of porous
586 polymeric nanofibers with surface-enriched iron oxide nanoparticles: composite filtration
587 materials for removal of metal cations. *Environ. Sci. Nano* **2018**, *5*, 669-681.
- 588 19. Peter, K. T.; Vargo, J. D.; Rupasinghe, T. P.; De Jesus, A.; Tivanski, A. V.; Sander, E.
589 A.; Myung, N. V.; Cwiertny, D. M., Synthesis, Optimization, and Performance
590 Demonstration of Electrospun Carbon Nanofiber–Carbon Nanotube Composite Sorbents
591 for Point-of-Use Water Treatment. *ACS Applied Materials & Interfaces* **2016**, *8*, 11431-
592 11440.
- 593 20. Kim, J.; Tsouris, C.; Oyola, Y.; Janke, C. J.; Mayes, R. T.; Dai, S.; Gill, G.; Kuo, L.-J.;
594 Wood, J.; Choe, K.-Y.; Schneider, E.; Lindner, H., Uptake of Uranium from Seawater by

- 595 Amidoxime-Based Polymeric Adsorbent: Field Experiments, Modeling, and Updated
596 Economic Assessment. *Industrial & Engineering Chemistry Research* **2014**, *53*, 6076-
597 6083.
- 598 21. Xu, X.; Zhang, H.; Ao, J.; Xu, L.; Liu, X.; Guo, X.; Li, J.; Zhang, L.; Li, Q.; Zhao, X.;
599 Ye, B.; Wang, D.; Shen, F.; Ma, H., 3D hierarchical porous amidoxime fibers speed up
600 uranium extraction from seawater. *Energy & Environmental Science* **2019**, *12*, 1979-
601 1988.
- 602 22. Horzum, N.; Shahwan, T.; Parlak, O.; Demir, M. M., Synthesis of amidoximated
603 polyacrylonitrile fibers and its application for sorption of aqueous uranyl ions under
604 continuous flow. *Chemical Engineering Journal* **2012**, *213*, 41-49.
- 605 23. Lu, G.; Johns, A. J.; Neupane, B.; Phan, H. T.; Cwiertny, D. M.; Forbes, T. Z.; Haes, A.
606 J., Matrix-Independent Surface-Enhanced Raman Scattering Detection of Uranyl Using
607 Electrospun Amidoximated Polyacrylonitrile Mats and Gold Nanostars. *Anal. Chem.*
608 **2018**, *90*, 6766-6772.
- 609 24. Sujata Mishra, M.; Chakravorty, V., Extraction of uranium(VI) by the binary mixture of
610 Aliquat 336 and PC88A from aqueous H₃PO₄ medium. *Hydrometallurgy* **1997**, *44* (3),
611 371-376.
- 612 25. Mishra, S.; Chakravorty, V.; Rao, P. R. V., Synergistic extraction of uranium(VI) and
613 americium(III) with binary mixtures of Aliquat 336 and PC 88A-TOPO from nitric-
614 sulfuric acid medium. *Journal of Radioanalytical and Nuclear Chemistry* **1995**, *201*, 325-
615 331.
- 616 26. Ramebäck, H.; Skållberg, M., Separation of neptunium, plutonium, americium and curium
617 from uranium with di-(2-ethylhexyl)-phosphoric acid (HDEHP) for radiometric and ICP-
618 MS analysis. *Journal of Radioanalytical and Nuclear Chemistry* **1998**, *235*, 229-234.
- 619 27. Ganguly, B., Spectroscopic investigation of uranium complexation in the reversed
620 micellar system HDEHP—n-heptane—water. *Journal of Photochemistry and*
621 *Photobiology A: Chemistry* **1990**, *51*, 401-409.
- 622 28. Aly, M. M.; Hamza, M. F., A Review: Studies on Uranium Removal Using Different
623 Techniques. Overview. *Journal of Dispersion Science and Technology* **2013**, *34*, 182-
624 213.
- 625 29. Eichrom. TRU Resin. <https://www.eichrom.com/eichrom/products/tru-resin/> (Accessed
626 September 15, 2019).
- 627 30. Kenkichi, N.; Keiji, N.; Utako, M., On the Mechanism of the Extraction of Uranyl Nitrate
628 by Tributyl Phosphate II. Infrared Study. *Bulletin of the Chemical Society of Japan* **1960**,
629 *33*, 894-898.
- 630 31. Ye, X.; Cui, S.; Almeida, V. d.; Khomami, B., Interfacial Complex Formation in Uranyl
631 Extraction by Tributyl Phosphate in Dodecane Diluent: A Molecular Dynamics Study.
632 *The Journal of Physical Chemistry B* **2009**, *113*, 9852-9862.
- 633 32. Crittenden, J. C., Trussell, R. R., Hand, D. W., Howe, K. J. and Tchobanoglous, G.,
634 Membrane Filtration. In *MWH's Water Treatment: Principles and Design*, J. C.
635 Crittenden, R. R. T., D. W. Hand, K. J. Howe and G. Tchobanoglous, Ed. 2012.
- 636 33. Froideval, A.; Del Nero, M.; Gaillard, C.; Barillon, R.; Rossini, I.; Hazemann, J. L.,
637 Uranyl sorption species at low coverage on Al-hydroxide: TRLFS and XAFS studies.
638 *Geochimica et Cosmochimica Acta* **2006**, *70*, 5270-5284.

- 639 34. Guibal, E.; Saucedo, I.; Roussy, J.; Le Cloirec, P., Uptake of uranyl ions by new sorbing
640 polymers: discussion of adsorption isotherms and pH effect. *Reactive Polymers* **1994**, *23*,
641 147-156.
- 642 35. Gunathilake, C.; Gorka, J.; Dai, S.; Jaroniec, M., Amidoxime-modified mesoporous silica
643 for uranium adsorption under seawater conditions. *Journal of Materials Chemistry A*
644 **2015**, *3*, 11650-11659.
- 645 36. Pekel, N.; Sahiner, N.; Guven, O., Thermodynamics of adsorption of uranyl ions onto
646 amidoximated poly(acrylonitrile)/poly(N-vinyl 2-pyrrolidone) interpenetrating polymer
647 networks. *Journal of Polymer Science Part B-Polymer Physics* **2004**, *42*, 986-993.
- 648 37. Hirotsu, T.; Katoh, S.; Sugasaka, K.; Seno, M.; Itagaki, T., Adsorption equilibrium of
649 uranium from aqueous $[\text{UO}_2(\text{CO}_3)_3]^{4-}$ solution on a polymer bearing amidoxime groups.
650 *Journal of the Chemical Society-Dalton Transactions* **1986**, 1983-1986.
- 651 38. Guillaumont, R.; Fanghanel, T.; Fuger, J.; Grenthe, I.; Neck, V.; Palmer, D. A.; Rand, M.
652 H., *Update on the Chemical Thermodynamics of Uranium, Neptunium, Plutonium,*
653 *Americium and Technicium*. Elsevier: Amsterdam, 2003; Vol. 5.
- 654 39. Kamp, S. D.; Morrison, S. J., Use of Chemical and Isotopic Signatures to Distinguish
655 Between Uranium Mill-Related and Naturally Occurring Groundwater Constituents.
656 *Ground Water Monit. Rem.* **2014**, *34*, 68-78.
- 657 40. Gorman-Lewis, D.; Burns, P. C.; Fein, J. B., Review of uranyl mineral solubility
658 measurements. *J. Chem. Thermodyn.* **2008**, *40*, 335-352.
- 659 41. Fujiwara, K.; Yamana, H.; Fujii, T.; Kawamoto, K.; Sasaki, T.; Moriyama, H., Solubility
660 product of hexavalent uranium hydrous oxide. *J. Nucl. Sci. Technol.* **2005**, *42*, 289-294.
- 661 42. Kapnisti, M.; Noli, F.; Misaelides, P.; Vourlias, G.; Karfaridis, D.; Hatzidimitriou, A.,
662 Enhanced sorption capacities for lead and uranium using titanium phosphates; sorption,
663 kinetics, equilibrium studies and mechanism implication. *Chem. Eng. J.* **2018**, *342*, 184-
664 195.
- 665 43. Cheng, K. L.; Ueno, K.; Imamura, T., *CRC Handbook of Organic Analytical Reagents,*
666 *Second Edition*. Taylor & Francis: New York, N.Y., 2017.
- 667 44. Kiwan, A. M.; Amin, R. S., Solvent-extraction of uranium (IV). 3. Extraction of
668 uranium(IV) by di-(2-ethylhexyl) phosphoric-acid from sulfuric-acid solutions. *Journal*
669 *of Inorganic & Nuclear Chemistry* **1974**, *36*, 2591-2593.
- 670 45. Riegel, M., Sorption of Natural Uranium on Weakly Basic Anion Exchangers. *Solvent*
671 *Extraction and Ion Exchange* **2017**, *35* (5), 363--375.
- 672 46. Quinn, J. E.; Ogden, M. D.; Soldenhoff, K., Solvent Extraction of Uranium (VI) from
673 Chloride Solutions using Cyphos IL-101. *Solvent Extraction and Ion Exchange* **2013**, *31*,
674 538-549.
- 675 47. St John, A. M.; Cattrall, R. W.; Kolev, S. D., Extraction of uranium(VI) from sulfate
676 solutions using a polymer inclusion membrane containing di-(2-ethylhexyl) phosphoric
677 acid. *Journal of Membrane Science* **2010**, *364*, 354-361.
- 678 48. Krestou, A.; Panias, D., Uranium (VI) speciation diagrams in the $\text{UO}_2^{2+}/\text{CO}_3^{2-}/\text{H}_2\text{O}$
679 system at 25 C. *The European Journal of Mineral Processing and Environmental*
680 *Protection* **2004**, *4*, 113-129.
- 681 49. Hu, L.; Yan, X.-W.; Yao, C.-G.; Deng, S.-Y.; Gao, X.-M.; Zhang, X.-J.; Shan, D.,
682 Preparation of amidoximated coaxial electrospun nanofibers for uranyl uptake and their
683 electrochemical properties. *Separation and Purification Technology* **2016**, *171*, 44-51.

- 684 50. Shao, D. D.; Li, Y. Y.; Wang, X. L.; Hu, S.; Wen, J.; Xiong, J.; Asiri, A. M.; Marwani,
685 H. M., Phosphate-Functionalized Polyethylene with High Adsorption of Uranium(VI).
686 *Acs Omega* **2017**, 2, 3267-3275.

687

Table of Contents Entry/Graphical Abstract

Johns *et al.* fabricates and demonstrates the performance of functionalized polymer nanofibers for treatment of uranium in contaminated drinking water.

